Science
AAAS

155,000 Years of West African Monsoon and Ocean Thermal Evolution

Syee Weldeab, *et al.*

Science **316**, 1303 (2007);
DOI: 10.1126/science.1140461

155,000 Years of West African Monsoon and Ocean Thermal Evolution

Syee Weldeab,[1]*† David W. Lea,[1] Ralph R. Schneider,[2] Nils Andersen[3]

A detailed reconstruction of West African monsoon hydrology over the past 155,000 years suggests a close linkage to northern high-latitude climate oscillations. Ba/Ca ratio and oxygen isotope composition of planktonic foraminifera in a marine sediment core from the Gulf of Guinea, in the eastern equatorial Atlantic (EEA), reveal centennial-scale variations of riverine freshwater input that are synchronous with northern high-latitude stadials and interstadials of the penultimate interglacial and the last deglaciation. EEA Mg/Ca-based sea surface temperatures (SSTs) were decoupled from northern high-latitude millennial-scale fluctuation and primarily responded to changes in atmospheric greenhouse gases and low-latitude solar insolation. The onset of enhanced monsoon precipitation lags behind the changes in EEA SSTs by up to 7000 years during glacial-interglacial transitions. This study demonstrates that the stadial-interstadial and deglacial climate instability of the northern high latitudes exerts dominant control on the West African monsoon dynamics through an atmospheric linkage.

The West African (WA) monsoon is an important component of the climate system because (i) it is part of the global monsoon system that regulates the moisture and heat budget of the atmosphere in low latitudes; (ii) it is sensitive to climate processes in the northern high latitudes and tropical oceans (*1*); and (iii), at a regional level, it is the main determinant of agricultural production in densely populated areas where the economy depends on subsistence agriculture. Thus, a deeper understanding of past WA monsoon dynamics and its controls is of pivotal importance to improving our knowledge of the monsoon system and assessing the impact of future climate change.

Previous studies of WA paleohydrology largely focused on the Holocene and the last deglaciation (*2*–*7*) and revealed alternating humid and dry conditions as reconstructed from lake-level fluctuations across the continent (*3*). These hydrological changes are thought to reflect the movement of the intertropical convergence zone (ITCZ) in close association with tropical SST and northern high-latitude climates (*2*, *4*). Because of the lack of a long, continuous, well-dated, and high-resolution record that includes independent and quantitative hydrological proxies, our understanding of the WA paleomonsoon and its teleconnections to global climate remains tenuous. To address these shortcomings, we present a 155,000-year reconstruction of WA monsoon precipitation variability at the centennial-to-millennial scale from marine sediment core MD03-2707 (02°30.11'N, 09°23.68'E, 1295 m water depth), which was recovered from the eastern part of the Gulf of Guinea in the EEA (Fig. 1).

Oceanographic setting and proxy records. The Gulf of Guinea is located in the eastern extension of the equatorial Atlantic warm tongue (*8*). In the upper 20 m of the water column, SST varies between 26° and 28.5°C (*8*). Freshwater input from the Sanaga and Niger rivers is the main factor determining modern sea surface salinity (SSS) variability in the eastern Gulf of Guinea (Fig. 1). The large volume of riverine runoff, combined with weak current and wind mixing (*9*, *10*), leads to markedly low SSS and a shallow halocline (20 to 30 m) (*8*) (Fig. 1). Our working hypothesis is that large-scale changes in past WA monsoon precipitation and riverine runoff are reflected in the isotopic composition of seawater and budget of dissolved Ba in Gulf of Guinea surface water, which is, in turn, archived in microfossils that accumulate in marine sediments. Because of the absence of coastal upwelling and strong local current mixing in the eastern part of the Gulf of Guinea (fig. S1), SST estimates likely reflect atmospheric conditions over the tropical Atlantic rather than advective signatures.

We measured Ba/Ca ratios, Mg/Ca ratios, and oxygen isotope composition ($\delta^{18}O$) in the tests (shells) of planktonic foraminifer *Globigerinoides ruber* (pink variety), which dwells in the upper 25 m of the water column, to infer past SSS and SST variation. MD03-2707 core sediment is 37.30 m long and covers the past 155,000 years (Fig. 2). The age model is described in (*10*). We applied Mg paleothermometry to obtain SST estimates using an established calibration equation (*11*). $\delta^{18}O$ in foraminiferal calcite ($\delta^{18}O_{calcite}$) is controlled by the calcification temperature and the $\delta^{18}O$ of seawater ($\delta^{18}O_{sw}$), which is controlled by salinity variation and continental ice volume. The $\delta^{18}O_{sw}$ is extracted by means of the Mg/Ca-based SST estimate with analyzed $\delta^{18}O$ and temperature-$\delta^{18}O_{calcite}$-$\delta^{18}O_{sw}$ relationship (*12*). $\delta^{18}O_{sw}$ is related linearly to salinity (*13*). However, changes in the origin of surface water and changes in $\delta^{18}O$ of riverine runoff make the use of the modern $\delta^{18}O_{sw}$-SSS relationship to determine paleo-SSS estimates uncertain.

Ba/Ca in planktonic foraminiferal calcite (Ba/Ca_{foram}) provides an innovative tool to assess past variability in regional riverine runoff (*14*). Seawater Ba (Ba_{sw}) concentrations at oceanic sites influenced by riverine runoff have a notably high inverse correlation to salinity, with high Ba and low salinity at sites closest to the river mouth (figs. S4 and S5) because dissolved Ba is high in riverine water and Ba desorbs from suspended sediments in estuaries (*15*, *16*). Laboratory experiments on living planktonic foraminifera demonstrate that Ba incorporation in foraminiferal calcite varies linearly with changes in Ba_{sw} concentration, independent of temperature changes within ~7°C (*17*). Therefore, the variation of Ba/Ca_{foram} is controlled by the Ba_{sw} concentra-

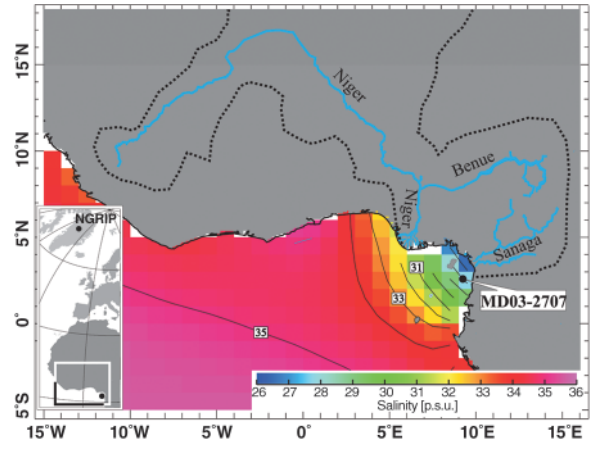

Fig. 1. Annual SSS in the Gulf of Guinea (*8*). Location of MD03-2707 (02°30.11'N, 09°23.68'E, 1295 m water depth) and drainage basin of Niger and Sanaga rivers (delineated by dotted line) are indicated. The Sanaga River, with an annual discharge of 77 km^3, drains a basin of 158,000 km^2 with the highest precipitation (10 mm/day) in the African continent (*23*); the catchment of the Niger River (2,400,000 km^2) integrates the largest part of WA monsoon area with annual runoff of almost 200 km^3 [data from Global Runoff Data Centre (http://grdc.bafg.de)]. Between June and September, intense monsoon precipitation (~180 to 240 mm/month) prevails over the catchments of the Niger and Sanaga rivers (*23*), resulting in a large freshwater input into the eastern part of the Gulf of Guinea.

[1]Department of Earth Science and Marine Science Institute, University of California, Santa Barbara, CA 93106–9630, USA. [2]Institut für Geowissenschaften, Universität Kiel, Germany. [3]Leibniz-Labor für Altersbestimmung und Isotopenforschung, Universität Kiel, Germany.

*Present address: Leibniz Institut für Meereswissenschaften an der Universität Kiel (IFM-GEOMAR), Germany.

†To whom correspondence should be addressed. E-mail: sweldeab@ifm-geomar.de

tion, and the temporal variation of Ba/Ca_{foram} provides valuable insights into changes in riverine freshwater input. In order to obtain an estimate of the past runoff-induced SSS variations, as recorded by Ba/Ca_{foram}, we use the modern Ba/Ca_{sw}-salinity relationship obtained off the Congo River (*15*) and Ba/Ca_{sw}-Ba/Ca_{foram} partition coefficient (*17*) to obtain a Ba/Ca_{foram}-SSS relationship (Fig. 2). Although our approach is supported by the observation that Ba_{sw} concentration in three different estuaries (fig. S5) affected by runoff from three major tropical rivers shows a high and similar degree of linear correlation with salinity (*10*), the Ba/Ca_{foram}-based SSS estimates should be regarded as a first-order estimate, because the Ba/Ca_{foram}-salinity relationship in the Gulf of Guinea is not yet established.

Holocene WA monsoon history. The Ba/Ca record is the most direct proxy of riverine runoff. Variability of $\delta^{18}O$ in *G. ruber* generally follows that of Ba/Ca, although the $\delta^{18}O$ fluctuations are less pronounced (Fig. 3). The close correspondence between Ba/Ca and $\delta^{18}O_{sw}$ indicates that the latter was largely controlled by riverine runoff throughout the record. The largest and most abrupt Ba/Ca rise in the Gulf of Guinea record occurs at ~11,460 years before the present and marks the end of the Younger Dryas (YD) chronozone and the beginning of the Holocene epoch. The increase of Ba/Ca from 1.4 to 1.8 μmol/mol, equivalent to an SSS change from 27 to 24 practical salinity units (psu), occurred within a few decades (~50 years) and points to an abrupt switch from relatively dry to extremely wet conditions and to a large northward expansion of the monsoonal rainfall front, as previously suggested by modeling studies (*18*, *19*) and paleoclimate data (*3*, *4*, *20*). The intensification of the monsoon in the earliest Holocene is consistent with Kutzbach's orbital forcing hypothesis, because perihelion occurred in early Northern Hemisphere summer at this time, resulting in enhanced summer insolation (*21*) and a seasonal warm tropical Atlantic (Fig. 3). Persistently high levels of Ba/Ca (~1.7 to 1.8 μmol/mol) for ~6300 years suggest that intense monsoon precipitation and high riverine runoff continued throughout the early and middle Holocene, with a salinity minimum of 23 psu, which is just 2 psu higher than the salinity limit (21 psu) for *G. ruber* growth (*22*). Superimposed on the generally extreme wet conditions during the middle and early Holocene (11,460 to 5100 yr B.P.) are several centennial-scale Ba/Ca fluctuations, including a prominent event close to 8200 yr B. P.

After ~5100 yr B.P., riverine Ba/Ca declined continuously, eventually attaining (at ~360 yr B.P.) an average value of 1 μmol/mol, which corresponds to an SSS estimate of 29 psu, which is equal to the modern annual SSS value at 10 to 25 m water depth over the core site (*8*). The gradual decline of riverine freshwater input over the late Holocene, as indicated by Ba/Ca and $\delta^{18}O$, is most likely associated with a continuous southward retreat of the monsoonal rainfall front from its northernmost expansion (~27°N) during the early and middle Holocene (*3*, *20*) to ~19°N at the present (*23*). This finding is consistent with the results of terrestrial studies from the drainage basin of the Niger River (*24*, *25*), suggesting that weakening and gradual southward displacement of monsoon precipitation were accompanied by gradual changes in vegetation.

We hypothesize that, in the absence of large northern high-latitude ice-sheet instabilities, WA Holocene monsoon precipitation is linked to Northern Hemisphere low-latitude summer insolation and EEA SST. In fact, high riverine runoff in the early and middle Holocene, as indicated by high Ba/Ca, is accompanied by high SST, and declining runoff occurred in parallel with decreasing SST throughout the late Holocene (Fig. 3). Furthermore, a comparison with other records of the global monsoon system indicates that the evolution of Holocene WA monsoon precipitation shares a close similarity with that of the Indian Ocean (*26*), the East Asian (EA) (*27*), and the South American monsoons (*28*), suggesting that declining Northern Hemisphere

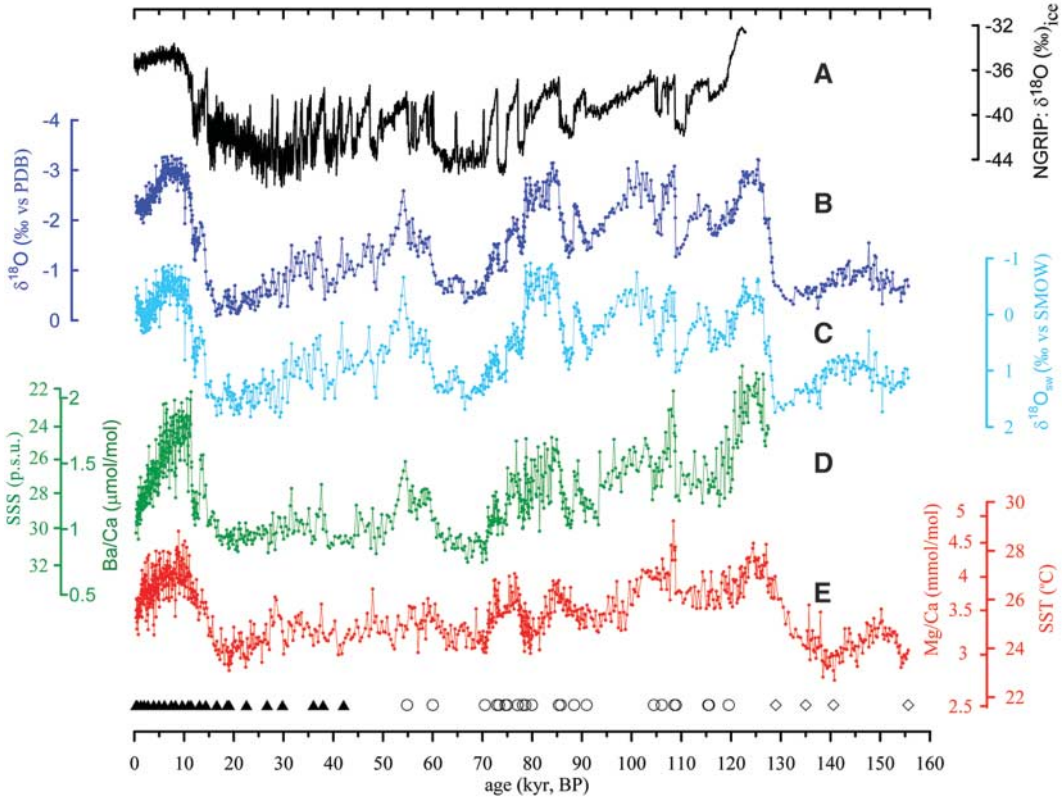

Fig. 2. Gulf of Guinea record based on trace element and $\delta^{18}O$ in tests of the shallow-dwelling planktonic foraminifer *G. ruber* (250 to 350 μm) from core MD03-2707. Proxy records in MD03-2707 are plotted versus calendar age [thousand years (kyr) B.P.] and compared with the $\delta^{18}O$ in ice ($\delta^{18}O_{ice}$) record of the NGRIP ice core (**A**) (*30*). $\delta^{18}O$ in the tests of *G. ruber* (**B**), $\delta^{18}O_{sw}$ (not corrected for changes in continental ice volume) (**C**), and Ba/Ca (μmol/mol) and Ba/Ca-based SSS estimates (**D**) are shown. PDB, Pee Dee belemnite; SMOW, standard mean ocean water. The Ba/Ca-based SSS estimate is calculated from the modern Ba_{sw}-salinity relationship obtained off the Congo River (*15*) and the partition coefficient for Ba incorporation in foraminifera of D_{Ba} = 0.147 [$Ba/Ca_{foram} = D_{Ba}\,(Ba/Ca_{sw})$] (*17*): SSS = [−7.47($Ba/Ca_{foram}$)] + 37.45; r^2 = 0.98; error estimate, ±0.41 psu (fig. S4). The Ba/Ca record between 122,000 and 127,500 yr B.P. might be slightly affected by diagenetic influence (*10*). (**E**) Mg/Ca (mmol/mol) and Mg/Ca-based SST estimates, where SST (°C) = 0.09^{-1}*ln[Mg/Ca(mmol/mol)/0.38] + 0.78 (*11*); SE estimate, ±1.2°C. Symbols along the *x* axis indicate age control points used for establishing the age model for MD03-2707 (*10*): Triangles indicate age control points as derived from a polynomial fit to individual calibrated ^{14}C-AMS ages (table S1 and fig. S3), and circles and diamonds are tie points obtained by the alignment of (i) the $\delta^{18}O$ record in (B) with the NGRIP $\delta^{18}O_{ice}$ record in (A) (*30*) and (ii) the benthic foraminiferal $\delta^{18}O$ record in MD03-2707 (fig. S2) with the "LR04" benthic foraminiferal $\delta^{18}O$ stack record (*49*), respectively (table S2).

summer solar insolation acted as a common control on the global monsoon system during the late Holocene (*29*).

Monsoon behavior during the last two deglaciations. Glacial Ba/Ca values are only slightly elevated over open-ocean Ba/Ca values (*15*), implying greatly reduced riverine runoff and SSS of ~32 psu (Figs. 2 and 3). Stable and low values give way to rising Ba/Ca after 16,430 yr B.P., indicating a gradual increase in runoff and precipitation. At 14,520 yr B.P., Ba/Ca rises sharply to peak values, corresponding to SSS of 26 psu during the Bølling-Allerød chronozone (B/A), indicating runoff levels similar to those of the early-late Holocene (~4000 yr B.P.). At the onset of the YD (~12,930 yr B.P.), Ba/Ca drops abruptly to 1.1 μmol/mol, indicating a collapse of riverine runoff and a salinity increase to 29 psu, most likely as a result of sharply reduced monsoonal precipitation. Sustained low Ba/Ca values coincident with the YD chronozone (~12,930 to 11,460 yr B.P.) suggest that dry conditions in western Africa lasted for ~1400 years.

The records of riverine runoff proxies in the Gulf of Guinea closely correlate with the North Greenland Ice Core Project (NGRIP) $\delta^{18}O$ record (*30*) during the last deglaciation (Fig. 3). Periods of warm air temperature over Greenland were associated with periods of high riverine runoff in WA, whereas cold conditions were associated with reduced runoff. Within age model uncertainties of ~±150 years, the onsets and terminations of the precipitation changes in the WA monsoon area during the B/A and YD are synchronous with the shift in the NGRIP record. This suggests a strong climate connection between northern high-latitude climate processes and WA monsoon precipitation, most likely due to synchronous latitudinal displacement of the polar front and the ITCZ.

In sharp contrast to the riverine runoff proxies, deglacial Mg/Ca ratios in the Gulf of Guinea record indicate a continuous SST rise from a glacial value of 24.1 ± 0.4°C (± 1 SD) between 23,000 and 19,000 yr B.P. to 27.2 ± 0.7°C between 11,000 and 8,500 yr B.P. This finding implies that deglacial air temperature instability over Greenland (*30*) was not matched by SST changes in the EEA. This observation, combined with SST reconstructions from the tropical western Atlantic (*31*), demonstrates that the YD did not leave a thermal imprint on the open-ocean equatorial Atlantic. Accordingly, the sharp YD cooling observed in the Cariaco Basin (*32*) reflects the sensitivity of this basin to northern high-latitude processes rather than a widespread open-ocean tropical Atlantic thermal event. It further implies that EEA SST was not the dominant control on deglacial WA monsoon precipitation variability. The continuous and gradual SST rise during the last deglaciation leads abrupt changes in monsoonal precipitation by ~2500 years. The penultimate deglacial is characterized by an even more pronounced lead-lag pattern, with gradually rising SST leading the rapid onset in monsoon intensification by ~7000 years. The finding that SST leads the deglacial monsoon onset by up to 7000 years suggests that regional SST rise was not the dominant control on deglacial WA monsoon evolution. Large-scale changes in atmospheric circulation linked to substantial reduction of the northern high-latitude ice sheets likely triggered the onset of monsoon intensification.

Glacial WA monsoon variability. Riverine runoff proxies suggest dry and relatively stable conditions during full glacial episodes in the WA monsoon area (Fig. 2). During the time intervals

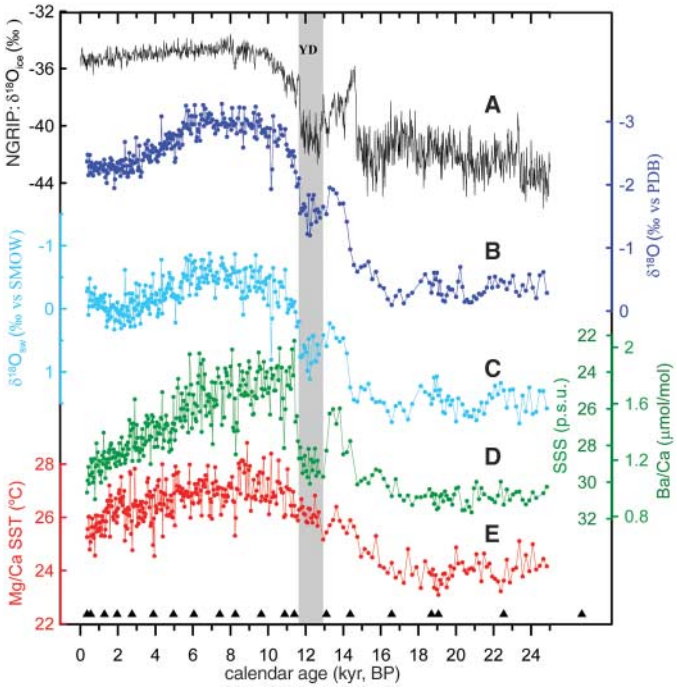

Fig. 3. Gulf of Guinea record over the past 25,000 years based on trace element and $\delta^{18}O$ in the tests of *G. ruber* from MD03-2707, in comparison with the $\delta^{18}O$ record of the NGRIP ice core (Greenland Ice Core Chronology 05) (*30*) (**A**). $\delta^{18}O$ in the tests of *G. ruber* (**B**), $\delta^{18}O_{sw}$ (not corrected for changes in continental ice volume) (**C**), Ba/Ca and Ba/Ca-based SSS estimates (**D**), and Mg/Ca-based SST estimates (**E**) are shown. Triangles along the *x* axis indicate age control points as driven from a polynomial fit to individual calibrated ^{14}C-AMS ages (table S1 and fig. S3). The gray bar marks the YD chronozone.

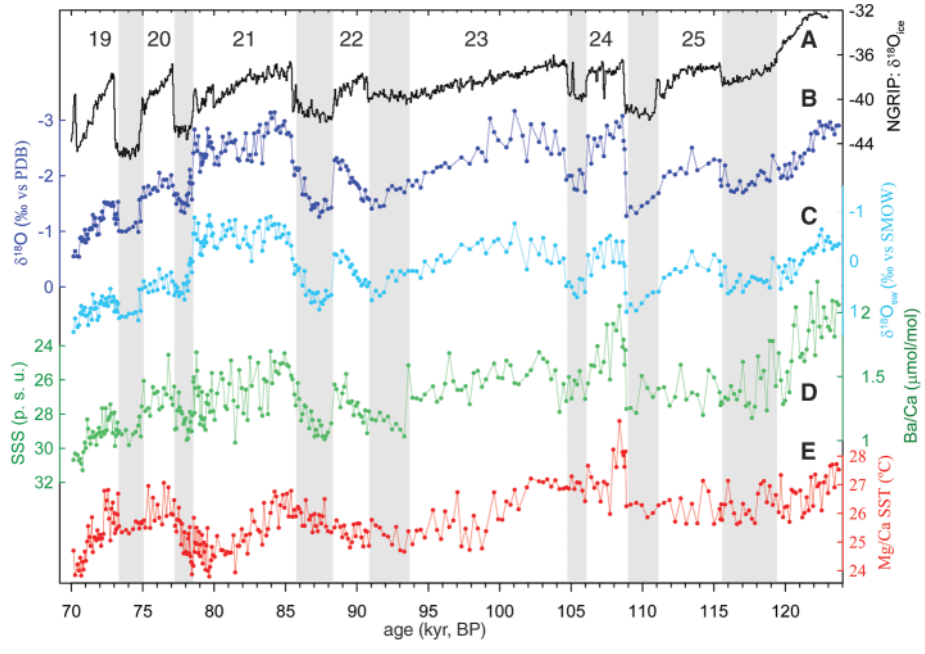

Fig. 4. Gulf of Guinea record covering the time interval from 65,000 to 123,000 yr B.P. based on trace element and $\delta^{18}O$ in the tests of *G. ruber* from MD03-2707, in comparison with $\delta^{18}O$ record of the NGRIP ice core (*30*) (**A**). $\delta^{18}O$ in the tests of *G. ruber* (**B**), $\delta^{18}O_{sw}$ (**C**), Ba/Ca (μmol/mol) and Ba/Ca-based SSS estimates (**D**), and Mg/Ca-based SST estimates (**E**) are shown. GIS identified in the $\delta^{18}O$ and Ba/Ca record of MD03-2707 are numbered ("19" to "25"), and associated GS are marked in gray.

from 19,000 to 51,000 and 61,500 to 70,000 yr B.P. [marine isotope stage 4 (MIS4)], Ba/Ca ratios are markedly low and stable, ranging from 0.9 to 1.1 μmol/mol, which corresponds to an estimated SSS of ~32 to 30 psu. Considering the effect of increasing continental ice volume on $\delta^{18}O_{sw}$ (*33*) from 52,000 through 19,000 yr B.P., the $\delta^{18}O_{sw}$ record corroborates the overall environmental conditions suggested by Ba/Ca, indicating low and stable riverine runoff and a severely weakened WA monsoon system. Starting at the beginning of the MIS4-MIS3 transition (~62,000 yr B.P.), Ba/Ca gradually increases and peaks at ~55,000 yr B.P. with a value of ~1.5 μmol/mol, which corresponds to ~26.5 psu and suggests less saline surface water during early MIS3 relative to that of the late Holocene.

Unlike the last deglacial and penultimate interglacial (Fig. 4), glacial WA riverine runoff, as recorded by Ba/Ca and $\delta^{18}O_{sw}$, did not fluctuate in concert with Greenland interstadials (GIS) and stadials (GS) (*30*). Assuming that our sample resolution sufficiently captures centennial- to millennial-scale hydrological changes in MIS3 and MIS2, the Gulf of Guinea record suggests that glacial boundary conditions dampened the response of the WA monsoon system to glacial GIS. This is in sharp contrast to the South American (*34*, *35*), Indian Ocean (*36*, *37*), and EA monsoon systems (*38*), which reveal strong coupling to the GIS events between 19,000 and 60,000 yr B.P.

We hypothesize that the extent to which the WA monsoon responds to submillennial extratropical forcing may depend on the initial summer position of the ITCZ that is determined by glacial and interglacial boundary conditions. During glacials and the second half of MIS3, the hydrological proxies suggest minimum runoff and severely reduced precipitation over WA. This is consistent with a wide-ranging southward ITCZ displacement over the Atlantic realm as evidenced by concomitant dry conditions in the Cariaco basin (*39*) and wet conditions in northeastern Brazil (*35*). We argue that the seasonal northward migration of the oceanic ITCZ, which was positioned over the EEA during the glacials and late part of MIS3, did not extend north of the east-west trending WA coast, and that the ITCZ response to glacial GIS warming was dampened by the large thermal inertia of the ocean.

WA monsoon variability during the penultimate interglacial. Hydrological proxies in the Gulf of Guinea record indicate numerous millennial-scale fluctuations in riverine freshwater input during the penultimate interglacial (MIS5) (Fig. 4). Both Ba/Ca and $\delta^{18}O_{sw}$ suggest enhanced riverine runoff at time intervals that correlate to GIS 19 through the Eemian and low runoff at the associated GS (GS 19 to GS 25) [as a result of diagenetic complications, Ba/Ca is not considered beyond 127,500 yr B.P. (*10*)]. Close examination also reveals that the relative amplitude of Ba/Ca and $\delta^{18}O$ changes in the Gulf of Guinea record correlating to GIS 19 and GIS 20 are less pronounced than those observed in the NGRIP record. We attribute this to the fact that both GIS 19 and GIS 20 occurred during the transition from interglacial (MIS5a) to glacial boundary conditions (MIS4), which, as argued above, appeared to dampen the WA monsoon response to extratropical influence. Some slight differences in the pattern of transitions also exist from stadial to interstadial and vice versa in the Gulf of Guinea record when compared with that of the NGRIP record (Fig. 4). GIS 23, for example, terminated abruptly as indicated by Ba/Ca in the MD03-2707 record; in the NGRIP record, the transition to GS 22 is gradual. The role of EEA SST in modulating the WA monsoon precipitation during MIS5 (Fig. 4) was most likely secondary. This observation suggests that although the general conditions of millennial-scale WA monsoon precipitation during the MIS5 were set by northern high-latitude climate conditions, the amplitude and abruptness of WA precipitation changes appear to be modulated by internal variability of the monsoon system or were preconditioned by low-latitude summer insolation.

EEA SST forcings. Major changes in EEA SST are recorded at glacial terminations I and II, equivalent to SST increases of 3.1 ± 0.8° and 3.7 ± 0.5°C, respectively (Figs. 2 and 5). The EEA SST record is also in phase with midsummer solar insolation at 15°N (*29*) (fig. S6), suggesting that the EEA is thermally sensitive to Northern Hemisphere low-latitude summer radiation, either through a monsoonal feedback (*21*) or because Mg/Ca-based SST estimates are weighted toward the boreal summer. The effect of orbital forcing in the EEA SST changes is best exemplified by the SST rise at 140,000 to 155,000 yr B.P. when atmospheric greenhouse gases and their associated radiative forcings were low, as indicated in the Vostok record (*40*) (fig. S6). Apart from the large SST changes during terminations (i.e., the 100,000-year cycles) and those related to precessional variance in summer insolation, a feature that stands out is a cooling of ~2°C between ~84,500 and 78,000 yr B.P. Comparison of EEA SST with the Vostok ice-core record (*40*) reveals that air temperature cooling over Antarctica and a decrease in atmospheric CO_2 also occurred at this time. This observation suggests that the decrease in EEA SST, as indicated by Mg/Ca, might relate to a broad-scale tropical cooling in response to greenhouse gas changes in the atmosphere. Major glacial-interglacial SST transitions in the EEA and elsewhere in the tropics (*41*–*43*) are paralleled by large changes in greenhouse gases as recorded in Antarctica ice cores (*40*). Radiative forcing associated with the increase in greenhouse gases during the glacial-interglacial transition has been estimated to give rise to an increase of ~2° to 3°C in tropical SST (*44*) and ~4° to 6°C in air temperature over Antarctica (*40*). If this estimate is correct, the EEA SST increase at termination I and II was largely a consequence of radiative forcing corresponding to greenhouse gas increases. The abrupt increase of atmospheric methane associated with the intensified global monsoon (Fig. 5) would have also enhanced greenhouse

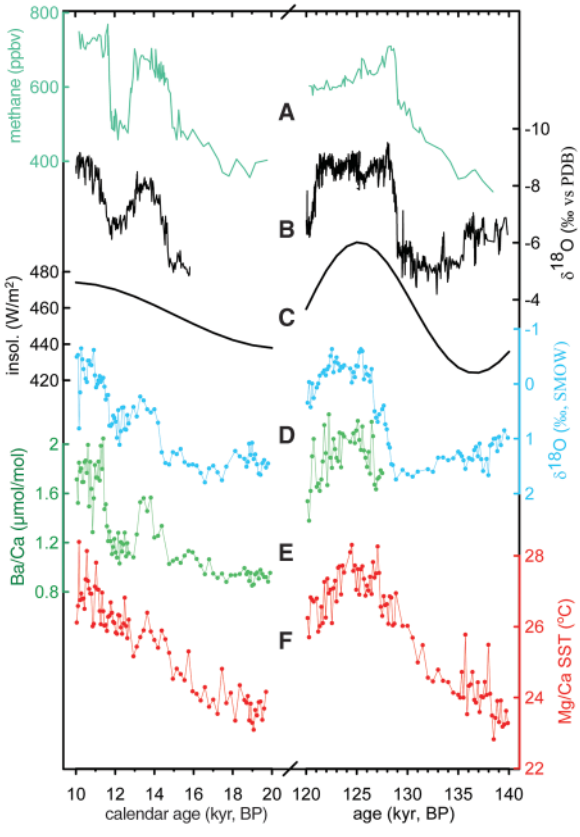

Fig. 5. Timing of deglacial onsets of the WA monsoon [as indicated by $\delta^{18}O_{sw}$ (**D**) and Ba/Ca (**E**)] and the Gulf of Guinea SST record during termination I and II (**F**), as compared with the EA monsoon record from Dongge Cave (**B**) (*27*, *46*), the midsummer solar insolation (insol.) at 15°N (*29*) (**C**), and changes in atmospheric methane concentration (**A**), as measured in the Greenland Ice Sheet Project 2 ice core (*47*) and in the Vostok ice core, Antarctica (*40*). ppbv, parts per billion per volume. The termination II Ba/Ca record is slightly affected by sedimentary contamination, and measurements older than ~127,000 yr B.P. are not shown (*10*). Abrupt monsoon WA and EA changes occurred late in the deglacial phase, whereas SSTs warmed relatively continuously and without abrupt shifts throughout the deglaciation. This observation suggests that the WA and EA monsoons acted in synchrony and supports the notion that the abrupt atmospheric methane increase associated with glacial terminations may have its source in monsoon areas (*46*, *48*).

forcing, thereby acting as a tropical feedback. Thus, EEA SST was mainly controlled by radiative forcing corresponding to the variation of atmospheric greenhouse gases (*40*) and orbital forcing (precession); submillennial ice-sheet instabilities in the northern high latitudes did not leave a strong imprint in the thermal evolution of the open-ocean tropical Atlantic, as has been previously observed in the Pacific (*45*). This strongly supports the general observation that thermal changes in the tropics primarily reflect greenhouse forcing and, to a lesser extent, orbital insolation changes.

WA monsoon in the context of the global monsoon system. The results of this study demonstrate the interplay and importance of several factors and forcings that govern the WA monsoon system at different time scales and boundary conditions. The role of low-latitude midsummer solar insolation and tropical SST in modulating the WA monsoon system is clearly evident, but millennial-scale extratropical influences can override tropical forcing. The major increase of deglacial WA monsoon precipitation coincides, within age model uncertainty, with the intensification of the EA monsoon (*27*, *46*) and rapid increase of atmospheric methane (*40*, *47*). This observation suggests that, during deglaciation, the WA and EA monsoons acted in synchrony and supports the notion that the abrupt atmospheric methane increase associated with glacial terminations may have its source in monsoon areas (*46*, *48*) (Fig. 5). However, the WA and EA monsoons responded differently to millennial-scale extratropical influence during the penultimate interglacial: The WA monsoon was weak during GIS events, while the EA monsoon largely followed insolation forcing (*27*). In contrast, during late MIS3 and MIS2, the WA monsoon did not vary strongly, while the EA monsoon varied in concert with GIS events. Land-ocean configuration and glacial-interglacial boundary conditions appear to exert constraints on how individual monsoon systems respond to millennial-scale northern high-latitude climate instabilities.

References and Notes

1. P. Camberlin, S. Janicot, I. Poccard, *Int. J. Climatol.* **21**, 973 (2001).
2. P. deMenocal, J. Ortiz, T. Guilderson, M. Sarnthein, *Science* **288**, 2198 (2000).
3. F. Gasse, *Quat. Sci. Rev.* **19**, 189 (2000).
4. S. Weldeab, R. R. Schneider, M. Kölling, G. Wefer, *Geology* **33**, 981 (2005).
5. M. R. Talbot, T. Johannessen, *Earth Planet. Sci. Lett.* **110**, 23 (1992).
6. A. T. Adegbie, R. Schneider, U. Röhl, G. Wefer, *Palaeogeogr. Palaeoclimatol. Palaeoecol.* **197**, 323 (2003).
7. T. M. Shanahan *et al.*, *Palaeogeogr. Palaeoclimatol. Palaeoecol.* **242**, 287 (2006).
8. S. Levitus, T. P. Boyer, *World Ocean Atlas 1994* (National Oceanic and Atmospheric Administration, National Environmental Satellite, Data, and Information Service, U.S. Department of Commerce, Washington, D.C., 1994), vol. 4.
9. G. Gu, R. F. Adler, *J. Clim.* **17**, 3364 (2004).
10. Materials and methods are available as supporting material on *Science* Online.
11. P. S. Dekens, D. W. Lea, D. K. Pak, H. J. Spero, *Geochem. Geophys. Geosyst.* **3**, 1022 (2002).
12. B. E. Bemis, H. Spero, J. Bijma, D. W. Lea, *Paleoceanography* **13**, 150 (1998).
13. G. A. Schmidt, *Paleoceanography* **14**, 482 (1999).
14. J. M. Hall, L.-H. Chan, *Paleoceanography* **19**, PA1017 (2004).
15. J. M. Edmond, E. D. Boyle, D. Drummond, B. Grant, T. Mislick, *Neth. J. Sea Res.* **12**, 324 (1978).
16. M. Coffey *et al.*, *Estuar. Coast. Shelf Sci.* **45**, 113 (1997).
17. D. W. Lea, H. Spero, *Paleoceanography* **9**, 445 (1994).
18. A. Ganopolski, C. Kubatzki, M. Clausen, V. Brovkin, V. Petoukhov, *Science* **280**, 1916 (1998).
19. Z. Liu, Y. Wang, R. Gallimore, M. Notaro, J. C. Prentice, *Geophys. Res. Lett.* **33**, L22709 (2006).
20. H. Kuhlmann, H. Meggers, T. Freudenthal, G. Wefer, *Geophys. Res. Lett.* **31**, L22204 (2004).
21. J. E. Kutzbach, Z. Liu, *Science* **278**, 440 (1997).
22. J. Bijma, W. W. Faber, C. Hemleben, *J. Foraminiferal Res.* **20**, 95 (1990).
23. J. E. Janowiak, P. Xie, *J. Clim.* **12**, 3335 (1999).
24. A. M. Lezine, J. C. Duplessy, J. P. Cazet, *Palaeogeogr. Palaeoclimatol. Palaeoecol.* **219**, 225 (2005).
25. U. Salzmann, P. Hoelzmann, I. Morczinek, *Quat. Res.* **58**, 73 (2002).
26. D. Fleitmann *et al.*, *Science* **300**, 1737 (2003).
27. D. Yuan *et al.*, *Science* **304**, 575 (2004).
28. G. H. Haug, K. A. Hughen, D. M. Sigman, L. C. Peterson, U. Röhl, *Science* **293**, 1304 (2001).
29. A. Berger, M. F. Loutre, *Quat. Sci. Rev.* **10**, 297 (1991).
30. K. K. Andersen *et al.*, *Nature* **431**, 147 (2004).
31. S. Weldeab, R. R. Schneider, M. Kölling, *Earth Planet. Sci. Lett.* **241**, 699 (2006).
32. D. W. Lea, D. K. Pak, L. C. Peterson, K. A. Hughen, *Science* **301**, 1361 (2003).
33. C. Waelbroeck *et al.*, *Quat. Sci. Rev.* **21**, 295 (2002).
34. R. G. Peterson, L. Stramma, *Prog. Oceanogr.* **26**, 1 (1991).
35. X. Wang *et al.*, *Nature* **432**, 740 (2004).
36. S. J. Burns, D. Fleitmann, A. Matter, J. Kramers, A. A. Al-Subbary, *Science* **301**, 1365 (2003).
37. H. Schulz, U. von Rad, H. Erlenkeuser, *Nature* **393**, 54 (1998).
38. L. Wang *et al.*, *Science* **294**, 2345 (2001).
39. L. C. Peterson, G. H. Haug, K. A. Hughen, U. Rohl, *Science* **290**, 1947 (2000).
40. J. R. Petit *et al.*, *Nature* **399**, 429 (1999).
41. D. W. Lea, D. K. Pak, H. J. Spero, *Science* **289**, 1719 (2000).
42. R. Saraswat, R. Nigam, S. Weldeab, A. Mackensen, P. D. Naidu, *Geophys. Res. Lett.* **32**, L24605 (2005).
43. R. R. Schneider, P. J. Müller, G. Ruhland, *Paleoceanography* **10**, 197 (1995).
44. D. W. Lea, *J. Clim.* **17**, 2170 (2004).
45. L. Stott, C. Pulsen, S. Lund, R. Thunell, *Science* **297**, 222 (2002).
46. M. J. Kelly *et al.*, *Palaeogeogr. Palaeoclimatol. Palaeoecol.* **236**, 20 (2006).
47. E. J. Brook, T. Sowers, J. Orchardo, *Science* **273**, 1087 (1996).
48. J. P. Severinghaus, T. Sowers, E. J. Brook, R. B. Alley, M. L. Bender, *Nature* **391**, 141 (1998).
49. L. Lisiecki, M. E. Raymo, *Paleoceanography* **20**, PA1003 (2005).

50. We thank G. L. Paradis for mass spectrometry operation, T. Guilderson and P. Grootes for accelerator mass spectrometry (AMS)–^{14}C dating, H.-H. Cordt, H. Gier, and H. Heckt for stable isotope measurements, Z. Liu for discussion, J. Dupak for sample preparation and discussion, and C. Rühlemann and E. Schefuß for shipboard help. R.R.S. thanks Institut Français pour la Recherche et la Technologie Polaires for Calypso coring through European Union grant HPRI-2001-00120. S.W. has been funded by the Deutsche Forschungsgemeinschaft (postdoctoral fellowship grant WE 2686/2-1) and D.W.L. by NSF (grants OCE0317611 and OCE0502609).

Supporting Online Material

www.sciencemag.org/cgi/content/full/316/5829/1303/DC1
Materials and Methods
Figs. S1 to S6
Tables S1 and S2
References

26 January 2007; accepted 12 April 2007
10.1126/science.1140461

Legumes Symbioses: Absence of *Nod* Genes in Photosynthetic Bradyrhizobia

Eric Giraud,[1]*† Lionel Moulin,[1] David Vallenet,[2] Valérie Barbe,[3] Eddie Cytryn,[4] Jean-Christophe Avarre,[1] Marianne Jaubert,[1] Damien Simon,[1] Fabienne Cartieaux,[1] Yves Prin,[1] Gilles Bena,[1] Laure Hannibal,[1] Joel Fardoux,[1] Mila Kojadinovic,[5] Laurie Vuillet,[1] Aurélie Lajus,[2] Stéphane Cruveiller,[2] Zoe Rouy,[2] Sophie Mangenot,[3] Béatrice Segurens,[3] Carole Dossat,[3] William L. Franck,[6] Woo-Suk Chang,[6] Elizabeth Saunders,[7] David Bruce,[7] Paul Richardson,[8] Philippe Normand,[9] Bernard Dreyfus,[1] David Pignol,[5] Gary Stacey,[6] David Emerich,[6] André Verméglio,[5] Claudine Médigue,[2] Michael Sadowsky[4]*†

Leguminous plants (such as peas and soybeans) and rhizobial soil bacteria are symbiotic partners that communicate through molecular signaling pathways, resulting in the formation of nodules on legume roots and occasionally stems that house nitrogen-fixing bacteria. Nodule formation has been assumed to be exclusively initiated by the binding of bacterial, host-specific lipochito-oligosaccharidic Nod factors, encoded by the *nodABC* genes, to kinase-like receptors of the plant. Here we show by complete genome sequencing of two symbiotic, photosynthetic, *Bradyrhizobium* strains, BTAi1 and ORS278, that canonical *nodABC* genes and typical lipochito-oligosaccharidic Nod factors are not required for symbiosis in some legumes. Mutational analyses indicated that these unique rhizobia use an alternative pathway to initiate symbioses, where a purine derivative may play a key role in triggering nodule formation.

Legume plants have developed symbiotic associations with specific soil bacteria, collectively referred to as the rhizobia, which allow plants to thrive and reproduce in nitrogen-poor environments. These plant-bacterial symbiotic associations typically result in the formation of root organs, termed nodules, in which the bacteria differentiate into nitrogen-fixing bacteroids. Initiation of nodule development involves molecular recognition between both symbiotic